

MIT Open Access Articles

Phosphoglycerate dehydrogenase diverts glycolytic flux and contributes to oncogenesis

The MIT Faculty has made this article openly available. **Please share** how this access benefits you. Your story matters.

Citation: Locasale, Jason W et al. "Phosphoglycerate Dehydrogenase Diverts Glycolytic Flux and Contributes to Oncogenesis." *Nature Genetics* 43.9 (2011): 869–874.

As Published: <http://dx.doi.org/10.1038/ng.890>

Publisher: Nature Publishing Group

Persistent URL: <http://hdl.handle.net/1721.1/76302>

Version: Author's final manuscript: final author's manuscript post peer review, without publisher's formatting or copy editing

Terms of use: Creative Commons Attribution-Noncommercial-Share Alike 3.0



Phosphoglycerate dehydrogenase diverts glycolytic flux and contributes to oncogenesis

Jason W. Locasale^{1,2*}, Alexandra R. Grassian⁵, Tamar Melman^{1,2}, Costas A. Lyssiotis^{1,2}, Katherine R. Mattaini³, Adam J. Bass^{4,8}, Gregory Heffron⁶, Christian M. Metallo⁷, Taru Muranen⁵, Hadar Sharfi^{1,2}, Atsuo T. Sasaki^{1,2}, Dimitrios Anastasiou^{1,2}, Edouard Mullarky^{1,2}, Natalie I. Vokes³, Mika Sasaki^{1,2}, Rameen Beroukhim^{4,8,11}, Gregory Stephanopoulos⁷, Azra H. Ligon^{4,10}, Matthew Meyerson^{4,8,9}, Andrea L Richardson^{4,10}, Lynda Chin^{4,12}, Gerhard Wagner⁶, John M Asara², Joan S. Brugge⁵, Lewis C. Cantley^{1,2*}, and Matthew G. Vander Heiden^{3,4*}

1 Department of Systems Biology, Harvard Medical School

2 Department of Medicine, Division of Signal Transduction, Beth Israel Deaconess Medical Center; Department of Medicine, Harvard Medical School

3 Koch Institute for Integrative Cancer Research, Department of Biology, Massachusetts Institute of Technology

4 Department of Medical Oncology, Dana Farber Cancer Institute, Harvard Medical School

5 Department of Cell Biology, Harvard Medical School

6 Department of Biochemistry and Molecular Pharmacology, Harvard Medical School

7 Department of Chemical Engineering Massachusetts Institute of Technology

8 Cancer Program, Broad Institute of MIT and Harvard

9 Center for Cancer Genome Discovery, Dana Farber Cancer Institute, Harvard
Medical School

10 Department of Pathology, Brigham and Women's Hospital

11 Department of Cancer Biology, Dana Farber Cancer Institute, Harvard Medical
School

12 Department of Dermatology, Harvard Medical School

* correspondence: Jlocasal@bidmc.harvard.edu, MVH@mit.edu, or
LCantley@hms.harvard.edu

Most tumors display increased glucose metabolism compared to that of normal tissues. The preferential conversion of glucose to lactate in cancer cells (the Warburg Effect) has been emphasized¹; however, the extent to which metabolic fluxes originating from glucose are utilized for alternative processes is poorly understood^{2,3}. Here we used a combination of mass spectrometry and NMR with stable isotope labeling to investigate the alternate pathways derived from glucose metabolism in cancer cells. We found that in some cancer cells, a relatively large amount of glycolytic carbon is diverted into serine and glycine biosynthesis through phosphoglycerate dehydrogenase (PHGDH). A bioinformatics analysis of 3131 human cancers revealed that the gene *PHGDH* at 1p12 is recurrently amplified in a genomic region of focal copy number gain most commonly found in melanoma in which amplification was associated with increased protein expression. Decreased PHGDH expression by RNA interference impaired growth and flux into serine metabolism in *PHGDH*-amplified cell lines. Increased expression was also associated with breast cancer subtypes and ectopic expression of PHGDH in mammary epithelial cells (MCF-10a) disrupted acinar morphogenesis, induced loss of polarity, and preserved the viability of the extracellular matrix-deprived cells, each being phenotypic alterations that may predispose cells to transformation. Our findings demonstrate that altered metabolic flux from glucose into a specific alternate pathway can be selected during tumor development and may contribute to the pathogenesis of human cancer.

Most tumors and cancer cell lines metabolize large amounts of glucose through a fermentative metabolism characterized by lactate production even in the presence of oxygen (aerobic glycolysis)¹. One idea is that aerobic glycolysis allows cancer cells to adapt metabolism to satisfy specific biosynthetic requirements^{2,3}. This hypothesis is buttressed by evidence indicating that the final step in glycolysis catalyzed by pyruvate kinase is inhibited in cancer cells^{4,5}. The selection for lower pyruvate kinase activity may allow glycolytic intermediates upstream of pyruvate kinase to be diverted into other metabolic pathways in cancer cells. However, it is not clear whether utilization of specific alternative pathways is necessary for cancer cell proliferation, nor whether differences in individual fluxes contribute to the development of cancers. Metabolomics in conjunction with stable isotope labeling of glucose allows for an unbiased interrogation of the pathways originating from glucose metabolism.

To better understand the diversity of glucose metabolism, we utilized sensitivity-enhanced NMR based 2-dimensional heteronuclear single quantum correlation spectroscopy (HSQC) to quantify steady state levels of glucose-derived metabolites in HEK293T cells following 24 hours of labeling with [U-¹³C]-glucose⁶. We discretized the spectra and computed the intensities of each resulting bin (Fig 1A, Table S1). Consistent with previous descriptions of glucose metabolism in cancer cells, two of the four highest intensity bins contained lactate peaks (Fig 1A). Surprisingly, a bin containing ¹³C-glycine was nearly as abundant as that containing ¹³C-lactate (Fig 1A). To determine whether this result was general to all cultured cells as has been suggested⁷⁻⁹, we carried out the [U-¹³C] glucose HSQC experiment

in two other exponentially growing cell lines: H1299 an epithelial lung cancer cell line and MCF-10a, a non-tumorigenic mammary epithelial cell line. In H1299 cells, we detected smaller relative quantities of ^{13}C labeled glycine (Fig 1B) while in MCF-10a cells, no ^{13}C labeled glycine was observed (Fig 1B). Together, these data indicate that cell lines display variability in glucose metabolism with differences in relative flux of glucose to glycine.

Glycine can be generated from glucose via diversion of the glycolytic intermediate, 3-phosphoglycerate (3PG), into the serine synthesis pathway and by the ultimate conversion of serine to glycine (Fig 1C)¹⁰. The first committed step in this pathway is the oxidation of 3PG to 3-phosphohydroxypyruvate (pPYR) by the enzyme phosphoglycerate dehydrogenase (PHGDH)¹¹. pPYR is transaminated by phosphoserine aminotransferase (PSAT) with glutamate as a nitrogen donor to form phosphoserine (pSER) and alpha-ketoglutarate (αKG), and pSER is then dephosphorylated by phosphoserine phosphatase (PSPH) to form serine (Fig 1C). Serine (SER) can be directly converted to glycine (GLY) by donation of a carbon into the folate pool. This pathway defines a branching point for 3PG from glycolysis, initialized by the enzymatic activity of PHGDH, that could otherwise be metabolized to pyruvate, alanine, and lactate. Serine and glycine are intermediates in pathways for the synthesis of other amino acids, as well as lipids and nucleic acids. Flux into this pathway has been observed in cancer cells but its cancer context, stoichiometry, requirement for cell growth, and potential to promote cell transformation have not been addressed⁷⁻⁹.

To further interrogate glucose metabolism in cells, we monitored the time course of conversion of [U- ^{13}C] glucose to other metabolites using targeted liquid chromatography/mass spectrometry (LC/MS)¹² in HEK293T cells. ^{13}C -labeled glucose incorporation into thirteen metabolites, in multiple pathways, was detected over the 30-minute time course (Fig 1D). The time required for labeled carbon to reach steady state in a pathway is a direct measurement of pathway flux. The data in Fig 1E reveal that ^{13}C incorporation into pSER (^{13}C -pSER) reaches steady state at a time scale comparable to the time for phosphoenolpyruvate (PEP) to reach steady state, suggesting that the relative fluxes are comparable. The ^{13}C -pSER labeling accompanied labeling of serine (Fig S1A) and labeling of serine was also confirmed using GC/MS by measuring pool sizes of incorporation of [α - ^{15}N] glutamine into amino acids (Fig S1B). These data are in agreement with our NMR experiments suggesting that a substantial fraction of glucose is diverted from 3PG into the serine and glycine biosynthetic pathway in these cells. To measure the total amount of glucose-derived serine, we cultured HEK293T cells in uniformly labeled ^{13}C glucose and measured metabolites from cell extracts using LC/MS. The total amount of labeled serine was found to be about one half, and this value was commensurate with the relative amount of glucose incorporation into nucleotides and nucleotide intermediates with the remaining fraction coming from other nutrients and salvage pathways (Fig 1F).

We verified expression of PHGDH by western blot (Fig 1G) and observed greater PHGDH protein expression in HEK293T cells compared to levels of expression observed in H1299 and MCF10a cells. Thus, the increased synthesis of

glycine from glucose in HEK293T cells is associated with higher PHGDH protein levels and the absence of its detection in MCF10a cells corresponds to approximately 30-fold lower protein expression.

The selective diversion of glucose metabolism into serine metabolism through PHGDH suggested that there might be a context in which selective pressure exists for tumors to increase PHGDH activity. One mechanism that can enhance PHGDH activity is an increase in the copy number at the genomic locus containing the *PHGDH* gene. We identified *PHGDH* in a study of a pooled analysis of somatic copy number alterations (SCNA) as a frequently amplified gene across 3131 cancer samples¹³. Compared to the false discovery rate (q-value) obtained from the background rate of SCNA in cancer, *PHGDH* was found in a peak of a region of chromosome 1p (1p12) that exhibits recurring copy number gain in 16% of all cancers (Supplementary Table S2). No known oncogenes are contained in the peak region of five genes (*PHGDH*, *REG4*, *HMGCS2*, *NBPF7*, *ADAM30*) at this locus. *PHGDH* is located in one of four peak regions of chromosome 1p ($q = 1.12e-9$) (Fig 2A, left). Two of the three high-scoring peaks contain the oncogenes *MYCL1* at 1p34 ($q = 1.7e-14$) and *JUN* at 1p32 ($q = 8.55e-7$) (Fig 2A, left). The copy number intensity of 150 cancers sorted by highest *PHGDH* copy number (Fig 2A, middle) was plotted along chromosome 1p showing that most samples containing *PHGDH* copy number gain have the genomic amplification localized near the 1p12 region. An inspection of the genomic region containing *PHGDH* (Fig 2A, right) illustrated the localized, amplification within the coding region of the *PHGDH* gene. Amplification was found

most commonly in melanoma (Fig S2) at 40% frequency in a three-gene peak region ($q = 1.93e-5$) with *HMGCS2* and *REG4*.

We first examined T.T. cells, an esophageal squamous cell carcinoma cell line that contained a highly focal copy number gain of *PHGDH*¹³ as determined by SNP array, and carried out fluorescence in situ hybridization (FISH) to verify copy number gain (Fig 2B). Focal copy number gain in *PHGDH* suggested that expression might be important for proliferation in these cells and stable PHGDH knockdown using shRNA reduced the proliferation rate (Fig 2B). To test whether the decreased proliferation was due to alterations in the ability to utilize the serine biosynthesis pathway, we created cell lines with decreased expression of downstream enzymes PSAT and PSPH and found that shRNA-mediated knockdown of these enzymes resulted in similar decreases in proliferation (Fig 2B).

Since *PHGDH* amplification in a single tumor type was most commonly found in melanoma, we assessed PHGDH expression and copy number gain in human melanoma tissue samples. Immunohistochemistry (IHC) was used to measure PHGDH expression in a tissue collection of human melanoma and high expression (IHC score > 1) was observed in 21% of the samples (Fig S3A, B). We then used FISH to probe relative *PHGDH* copy number in a subset of 42 of these samples (Fig S3C). PHGDH copy number gain was observed in 21 of the 42 samples; however, 16 of these samples also contained an equal increased number of copies of a probe sequence adjacent to the centromere, indicating either polysomy or that the amplified region also contained the pericentromeric region of chromosome 1p. Five tumors exhibited copy number gain with the number of copies greater than the

number of pericentromeric probes (Fig 2C). It was observed that each sample with relative gain had high expression by IHC (Fig 2C), indicating that *PHGDH* copy number gain and amplification associates with significant protein overexpression in human melanoma ($p = 0.0045$, Fisher's exact test, two-tailed).

We next investigated whether melanoma cell lines containing *PHGDH* copy number gain would be sensitive to decreased expression of *PHGDH*. Three tumor-derived human melanoma cell lines (WM1266-3, Malme-3M, and SK-Mel28) with 1p12 gain were obtained along with two additional melanoma cell lines (Gak, Carney)¹⁴. Pairs of cell lines containing shRNA targeting *PHGDH* and GFP as a control were created for each cell line (Fig 3A, left). Each of the amplified cell lines showed decreased proliferation in contrast to the non-amplified cell lines that showed no difference in proliferation upon *PHGDH* knockdown indicating that the growth of the amplified cell lines is differentially sensitive to *PHGDH* knockdown (Fig 3A, right). To verify that high expression leads to metabolic flux through the serine pathway, we measured the relative incorporation of ¹³C serine from [U-¹³C] glucose and found that each of the amplified cell lines had appreciable glycolytic flux into serine (Fig 3B). One cell line that did not contain the amplification, Carney, had high expression of *PHGDH* and high flux into serine synthesis (Fig 3A,B). Previous studies of oncogene addiction have shown that loss of cancer cell proliferation correlates with the presence of a genetic lesion and not with gene expression^{15,16}. Consistent with these findings, it was observed that *PHGDH* knockdown had no effect on growth in Carney cells despite increased serine pathway flux (Fig 3A).

We then asked whether knockdown of PHGDH to levels that impair proliferation also affects metabolism. Metabolomics was carried out on SK-Mel28 cells using targeted LC/MS to profile metabolite levels with or without knockdown of PHGDH. Consistent with affecting the activity of glucose flux into serine metabolism, PHGDH knockdown reduced pSER levels in Sk-Mel28 cells (Fig 3C) and globally altered metabolite levels including the levels of many intermediates in glycolysis (Fig 3D, Supplementary Table S3). Increased levels of metabolites in glycolysis near the point of diversion into serine metabolism were observed (Fig 3E) confirming that the level of PHGDH expression alters glucose metabolism in SkMel-28 cells by modulating the entry of glycolytic metabolites into serine metabolism.

While copy number gain at the *PHGDH* genomic locus is one mechanism to divert flux into serine biosynthesis, other mechanisms to elevate PHGDH expression likely exist and may be important in specific cancer contexts. Recently, a study in breast cancer found enhanced high PHGDH mRNA expression was associated with poor prognosis in breast cancer¹⁷. Copy number gain was also found in breast cancer but at low frequency and in a broad peak region. To further investigate the role of PHGDH in breast cancer, we first carried out a bioinformatics analysis of multiple tumor microarray data sets in breast cancer and found strong associations ($p < 1e-4$) with several clinical parameters in breast cancer (Fig S4, Supplementary Table S4). These data suggest that PHGDH expression segregated with specific cancer subtypes. For validation, PHGDH protein expression in 106 human breast cancer tumor samples was assessed by IHC (Fig S5A) and correlated with mRNA expression (Fig S5B). It was found that high PHGDH expression (IHC score > 1) was

associated with distinct subtypes of breast cancer, as expression correlated with both triple-negative¹⁸ ($p = 0.002$, Fisher's exact, two tailed) and basal subtypes ($p = 0.004$, Fisher's exact, two tailed) (Fig S6). However, there was no association with general parameters such as metastasis as was previously reported¹⁷ or with tumor size also suggesting that expression is subtype specific. Consistent with a reliance of a subset of breast cancers on PHGDH, protein expression was required for growth in a panel of three (BT-20, SK-BR-3, MCF-7) breast cancer cell lines (including the BT-20 cell line that carries amplification) to differing extents (Fig S7A). Furthermore, decreased PHGDH expression decreased pSer levels in PHGDH amplified BT-20 cells. In contrast, non-tumorigenic breast epithelial cells (MCF-10a) did not require PHGDH for growth (Fig S7A), did not exhibit alterations in glycolysis upon shRNA knockdown of PHGDH (Fig S7B) and exhibited no detectable labeling of pSER from glucose (Fig S7C).

We therefore questioned whether ectopic expression of PHGDH would increase flux of glucose to serine and have any phenotypic consequences. MCF-10a cells are non-tumorigenic and, when grown in reconstituted basement membrane (™Matrigel) form structures resembling many features of mammary acini. These acini-like structures are polarized and characterized by a hollow lumen due to selective apoptosis of the inner, matrix-deprived cells. This model has been used to monitor alterations in growth arrest, polarization, invasive behavior and other disruptions of normal morphogenesis that resemble changes associated with different stages of tumor formation¹⁹. PHGDH was expressed in MCF-10a cells using a tetracycline-inducible expression vector and treatment of the engineered MCF-

10A cells with increasing concentrations of doxycycline induced expression of PHGDH (Fig 4A). pSER levels were elevated to detectable levels in cells treated with 1 μ g/ml doxycycline indicating an increase in pathway activity (Fig 4B) that was confirmed with GC/MS that measured an increase in Serine and Glycine synthesis (Fig S7D).

We seeded PHGDH-expressing MCF-10A cells in TMMatrigel reconstituted basement membrane and monitored the structures at increasing doses of doxycycline using confocal microscopy and immunofluorescence staining of nuclei (DAPI) and extracellular matrix (laminin-5) (Fig 4C). In the absence of doxycycline, MCF-10A cells formed hollow, acini-like structures as previously reported²⁰(Fig 4C). In contrast, PHGDH-expressing cells formed disorganized structures lacking a lumen (Fig 4C). The PHGDH-expressing cells also exhibited large, abnormal nuclear morphologies, failed to orient in a uniform fashion adjacent to the basal acinar membrane, and displayed enhanced proliferation (Fig 4D). The majority of the control acini were either clear or mostly clear, whereas PHGDH expression dramatically increased the percentage of acini that scored as mostly filled or filled in a dose dependent manner (Fig. 4E). An activity-compromised mutant PHGDH (V490M)²¹ showed decreased luminal filling (Fig 4F and S7E). In addition, MCF-10A acini with ectopic expression of wild-type but not mutant PHGDH commonly displayed mislocalization of the golgi apparatus indicating loss of apical polarity (Fig. 4F). These results indicate that PHGDH expression alters glucose metabolism, disrupts luminal organization and polarity and preserves the viability of the inner,

matrix-deprived cells to survive in an anchorage-independent fashion. Importantly, these phenotypes depend on the catalytic activity of PHGDH.

Although numerous studies have correlated oncogenesis with changes in cell metabolism, only a few studies have suggested that genetic aberrations in metabolic genes are capable of driving tumorigenesis²². Oncogenic mutations in the metabolic enzyme isocitrate dehydrogenase have recently been described²³. These mutations result in production of a metabolite not normally produced in cells²⁴, suggesting that altered metabolic flux may promote oncogenesis. Here we show that PHGDH, a focus of recurrent genomic amplification, diverts glycolysis into a specific biosynthetic pathway and that this change in metabolism can be selected for in the development of human cancer.

The diversion of glycolytic flux into *de novo* serine biosynthesis has a multitude of biological consequences. Metabolic pathways downstream of serine metabolism contribute to growth-promoting biosynthesis and metabolic signaling functions from the folate pool, amino acid, and lipid intermediates, and redox regulation^{20,25-27}. In addition, the process of diverting fluxes from 3PG out of glycolysis confers several advantages for cell growth. These include limiting ATP production, direct alterations in cellular redox status from the oxidation of 3PG, and the generation of α KG from glutamate, all of which are reported to benefit cell growth through multiple mechanisms²⁸⁻³⁰. Since the consequences of *PHGDH* amplification and increased glucose flux into serine metabolism are numerous, multi-factorial, and comparable to the number of processes affected by classic oncogenes such as *KRAS*, it is not likely that a single biological mechanism

contributes to cell transformation downstream of *PHGDH* amplification.

Nevertheless, the observation that a genetic lesion can function to directly alter metabolic flux out of glycolysis provides multiple avenues for further inquiry and demonstrates that alterations in metabolism beyond increased lactate production are important events in the development of cancer.

Acknowledgements

Microscopy data for this study were acquired and analyzed in the Nikon Imaging Center at Harvard Medical School. JWL was supported by postdoctoral fellowships from the NIH and the American Cancer Society. ARG is a recipient of an NSF Graduate Research Fellowship. LCC and JSB were supported by grants from NIH and NCI. MVH was supported by grants from the NIH, NCI, and from the Burrough's Wellcome Fund. We thank Natalie Vena for technical assistance with the FISH analysis and Kaitlyn Webster and Inaira Carrecedo for help with Immunohistochemistry. We thank Josh Rabinowitz, Arkaitz Carrecedo, and Shyh-Chang Ng for helpful comments on the manuscript.

Figure Captions

Figure 1 - Observation of glycolytic metabolism being diverted into serine and glycine metabolism

a.) Spectral bins of [^1H , ^{13}C] HSQC NMR of [$\text{U-}^{13}\text{C}$] glucose-labeled cell extracts sorted by intensity in standard units (z-score). Four highest intensity peaks correspond to

metabolites lactate, alanine, and glycine respectively. b.) Relative intensity ^{13}C glycine peak normalized to an internal 50mM DSS standard in HEK293T, H1299, and MCF-10a cells. c.) Schematic of diversion of glucose metabolism into serine and glycine metabolism at the 3-phosphoglycerate (3PG) step through PHGDH. d.) Time (0, 5, 10, 15, 30 minutes) courses of U- ^{13}C labeling intensities of thirteen metabolites from [U- ^{13}C] glucose labeling experiments measured with targeted LC/MS relative to baseline level at time zero. e.) Comparison of 3-phosphoserine (pSER) and phosphoenolpyruvate (PEP) labeling kinetics of [U- ^{13}C] glucose relative to baseline level at time zero with targeted LC/MS. f.) Relative glucose flux into serine biosynthesis measured by steady-state labeling of [U- ^{13}C] glucose into serine with targeted LC/MS. The fraction of labeled to unlabeled glucose-derived metabolites $^{13}\text{C}/(^{12}\text{C}+^{13}\text{C})$ ion intensities (glucose incorporation) is plotted for 12 metabolites. Serine is compared with respect to the glucose-labeled fraction of downstream nucleotides and other nucleotide precursors. g.) Relative protein levels (as determined by western blot analysis) of PHGDH in HEK293T, H1299, and MCF-10a cells with a Beta-actin (Actin) loading control shown below the PHGDH band. Quantitation relative to the levels in MCF-10a cells of the total intensity of the PHGDH band relative to the Actin band is shown above.

Figure 2 - *PHGDH* amplification in human cancers and requirement for proliferation

a.) Global survey of *PHGDH* copy number intensity across 3131 cancers. (left) Plot significance of amplifications (FDR q-value) along chromosome 1p (from Telomere to Centromere) across 3131 samples. Candidate oncogenes (TP73, MYCL1, and JUN)

in three peak regions and corresponding FDR q-values are shown. FDR q-value of PHGDH is shown in the fourth peak region. (middle) Copy number intensity along chromosome 1p of 150 cancers containing highest intensity of *PHGDH* amplification that illustrates the localized intensity near the region of *PHGDH*. Blue indicates deleted region, white indicates neutral region and red indicates amplified region. (right) Magnification of 4MB region containing *PHGDH*. Solid line indicates chromosome position of PHGDH coding region. Ratios of ion intensities (fold change) are plotted. b.) Relative cell numbers of T.T. cells upon knockdown with respect to shGFP of GFP, PHGDH, PSAT, and PSPH. Error bars represent the standard deviation of n =3 independent measurements. (below) Interphase FISH analysis showing *PHGDH* copy number gain in T.T. cells. The green probe maps to 1p12 and includes the *PHGDH* coding sequence. The red probe maps to the pericentromeric region of chromosome1 (1p11.2-q11.1). (below) Relative protein levels of PHGDH, PSAT, and PSPH (as determined by western blot analysis) in T.T. cells following expression of an shRNA against GFP (shGFP), PHGDH (shPHGDH), PSAT (shPSAT), and PSPH (shPSPH) respectively. c.) PHGDH protein expression and copy number gain in three representative human tissue samples. (upper) PHGDH expression was assessed in tumor samples using Immunohistochemistry (IHC). Nuclei are shown in blue (hematoxylin) and PHGDH antibody staining is shown in brown (3-3'-Diaminobenzidine [DAB]). (lower) panels contain interphase FISH analysis that was carried out as in Fig 2B in matched samples to assess copy number (green) relative to the pericentromeric probe (red).

Figure 3 – Growth dependence of PHGDH expression and altered serine metabolism in PHGDH-amplified human melanoma cells

a.) Growth assay of stable cell lines containing shGFP or shPHGDH in five human melanoma cell line. Three (WM266-3, Malme-3M (Malme), and SkMel-28 (Sk28) contain 1p12 copy number gain and two (GAK, Carney) other melanoma cell lines are considered. (left) Western blot analysis of protein levels of PHGDH and corresponding protein levels of Actin shown as a loading control. (right) Cell numbers for shGFP and shPHGDH normalized to shGFP are plotted for each cell line. Error bars were obtained from the standard deviation of $n = 3$ independent measurements. b.) Relative amount of glucose flux into serine biosynthesis measured by steady-state labeling of [U- ^{13}C] glucose into serine with targeted LC/MS. The fraction of labeled to unlabeled glucose-derived serine to total serine, $^{13}\text{C}/^{12}\text{C} + ^{13}\text{C}$, (serine incorporation) is measured in each of the five cell lines. Error bars were obtained from the standard deviation of $n = 3$ independent measurements. c.) Relative ion intensities of 3-phosphoserine (pSer) in control (shGFP) and knockdown (shPHGDH) cells normalized to intensity in knockdown shGFP cells (pSer/shGFP). Error bars were obtained from the standard deviation of $n = 3$ independent measurements. d.) Scatter plot of the ratio of intensities (fold change), versus p value (student's t-test) of shPHGDH relative to shGFP in Sk-Mel28 cells. e.) Ratio of intensities (fold change) of glycolytic intermediates upon PHGDH knockdown (shPHGDH) relative to (shGFP) in Sk-Mel28 cells. Error bars were obtained from propagation of error of the standard deviation from three independent measurements.

Figure 4 – Enhanced PHGDH expression in human breast cancer and ectopic expression of PHGDH in ductal morphogenesis.

a.) Protein expression of PHGDH by western blot analysis with Actin as loading for three concentration of Doxycycline (0 μ g/ml, 1 μ g/ml, 2 μ g/ml). b.) pSER integrated intensities in -Dox (0 μ g/ml) and +Dox (1 μ g/ml). c.) Confocal images of DAPI (Blue), Laminin 5 (Green). Representative images from four acini from MCF-10A cells expressing doxycycline-inducible PHGDH without doxycycline (-Dox) or 1 μ g/ml doxycycline (+Dox). d.) Enhanced proliferation in the interior of PHGDH-expressing acini. Representative images from acini from MCF-10A cells expressing doxycycline-inducible PHGDH without doxycycline (No Dox) or 1 μ g/ml doxycycline (1 μ g/ml Dox). Confocal images of MCF-10A cells under the same conditions as in 4C with DAPI (Blue) and the proliferation marker Ki67 (Red). e.) Quantification of acinar filling for 0 μ g/ml, 1 μ g/ml, and 2 μ g/ml Dox. Each acini was scored as filled, mostly filled, mostly clear, and clear. These data are representative of multiple independent measurements. f.) Loss of apical polarity in PHGDH-expressing cells. Confocal images of MCF-10A cells under the same conditions as in 4C with DAPI (Blue) and Golgi Apparatus (Green). Solid, white arrows indicate cells displaying oriented golgi apparatus. Dashed, yellow arrows indicate cells exhibiting loss of polarity. Acini with ectopic expression of wild type, but not mutant V490M, PHGDH commonly display mislocalized golgi apparatus, indicative of a lack of cell polarity.

1. Warburg, O., Posener, K. & Negelein, E. Ueber den Stoffwechsel der Tumoren *Biochemische Zeitschrift* **152**, 319-344 (1924).
2. Vander Heiden, M.G., Cantley, L.C. & Thompson, C.B. Understanding the Warburg effect: the metabolic requirements of cell proliferation. *Science* **324**, 1029-33 (2009).
3. Deberardinis, R.J., Lum, J.J., Hatzivassiliou, G. & Thompson, C.B. The biology of cancer: metabolic reprogramming fuels cell growth and proliferation. *Cell Metab* **7**, 11-20 (2008).
4. Christofk, H.R., Vander Heiden, M.G., Wu, N., Asara, J.M. & Cantley, L.C. Pyruvate kinase M2 is a phosphotyrosine-binding protein. *Nature* **452**, 181-6 (2008).
5. Christofk, H.R. et al. The M2 splice isoform of pyruvate kinase is important for cancer metabolism and tumour growth. *Nature* **452**, 230-3 (2008).
6. Bodenhausen, G. & Ruben, D.J. NATURAL ABUNDANCE N-15 NMR BY ENHANCED HETERONUCLEAR SPECTROSCOPY. *Chemical Physics Letters* **69**, 185-189 (1980).
7. Bismut, H., Caron, M., Coudraylucas, C. & Capeau, J. GLUCOSE CONTRIBUTION TO NUCLEIC-ACID BASE SYNTHESIS IN PROLIFERATING HEPATOMA-CELLS - A GLYCINE-BIOSYNTHESIS-MEDIATED PATHWAY. *Biochemical Journal* **308**, 761-767 (1995).
8. Snell, K., Natsumeda, Y. & Weber, G. THE MODULATION OF SERINE METABOLISM IN HEPATOMA 3924A DURING DIFFERENT PHASES OF CELLULAR PROLIFERATION IN CULTURE. *Biochemical Journal* **245**, 609-612 (1987).
9. Kit, S. THE BIOSYNTHESIS OF FREE GLYCINE AND SERINE BY TUMORS. *Cancer Research* **15**, 715-718 (1955).
10. De Koning, T.J. et al. L-serine in disease and development. *Biochemical Journal* **371**, 653-661 (2003).
11. Achouri, Y., Rider, M.H., VanSchaftingen, E. & Robbi, M. Cloning, sequencing and expression of rat liver 3-phosphoglycerate dehydrogenase. *Biochemical Journal* **323**, 365-370 (1997).
12. Lu, W., Bennett, B.D. & Rabinowitz, J.D. Analytical strategies for LC-MS-based targeted metabolomics. *Journal of Chromatography B-Analytical Technologies in the Biomedical and Life Sciences* **871**, 236-242 (2008).
13. Beroukhi, R. et al. The landscape of somatic copy-number alteration across human cancers. *Nature* **463**, 899-905 (2010).
14. Greshock, J. et al. A comparison of DNA copy number profiling platforms. *Cancer Research* **67**, 10173-10180 (2007).
15. Slamon, D.J. et al. HUMAN-BREAST CANCER - CORRELATION OF RELAPSE AND SURVIVAL WITH AMPLIFICATION OF THE HER-2 NEU ONCOGENE. *Science* **235**, 177-182 (1987).
16. Luo, J., Solimini, N.L. & Elledge, S.J. Principles of Cancer Therapy: Oncogene and Non-oncogene Addiction. *Cell* **136**, 823-837 (2009).
17. Pollari S, K.S., Edgren H, Wolf M, Kohonen P, Sara H, Guise T, Nees M, Kallioniemi O. Enhanced serine production by bone metastatic breast cancer cells stimulates osteoclastogenesis. *Breast Cancer Res Treat.* (2010).

18. Foulkes, W.D., Smith, I.E. & Reis-Filho, J. Triple-Negative Breast Cancer. *New England Journal of Medicine* **363**(2010).
19. Debnath, J. & Brugge, J.S. Modelling glandular epithelial cancers in three-dimensional cultures. *Nature Reviews Cancer* **5**, 675-688 (2005).
20. Schafer, Z.T. et al. Antioxidant and oncogene rescue of metabolic defects caused by loss of matrix attachment. *Nature* **461**, 109-U118 (2009).
21. Tabatabaie, L. et al. Novel Mutations in 3-Phosphoglycerate Dehydrogenase (PHGDH) Are Distributed Throughout the Protein and Result in Altered Enzyme Kinetics. *Human Mutation* **30**, 749-756 (2009).
22. Thompson, C.B. Metabolic enzymes as oncogenes or tumor suppressors. *N Engl J Med* **360**, 813-5 (2009).
23. Parsons, D.W. et al. An integrated genomic analysis of human glioblastoma multiforme. *Science* **321**, 1807-12 (2008).
24. Dang, L. et al. Cancer-associated IDH1 mutations produce 2-hydroxyglutarate. *Nature* **462**, 739-U52 (2009).
25. Teperino, R., Schoonjans, K. & Auwerx, J. Histone Methyl Transferases and Demethylases; Can They Link Metabolism and Transcription? *Cell Metabolism* **12**, 321-327.
26. Nomura, D.K. et al. Monoacylglycerol Lipase Regulates a Fatty Acid Network that Promotes Cancer Pathogenesis. *Cell* **140**, 49-61.
27. Hara, K. et al. Amino acid sufficiency and mTOR regulate p70 S6 kinase and eIF-4E BP1 through a common effector mechanism. *Journal of Biological Chemistry* **273**, 14484-14494 (1998).
28. Vander Heiden, M.G. et al. Evidence for an Alternative Glycolytic Pathway in Rapidly Proliferating Cells. *Science* **329**, 1492-1499 (2010).
29. Locasale, J.W. & Cantley, L.C. Altered metabolism in cancer. *Bmc Biology* **8**, 3.
30. Eng, C.H., Yu, K., Lucas, J., White, E. & Abraham, R.T. Ammonia Derived from Glutaminolysis Is a Diffusible Regulator of Autophagy. *Science Signaling* **3**, 9.
31. Debnath, J., Muthuswamy, S.K. & Brugge, J.S. Morphogenesis and oncogenesis of MCF-10A mammary epithelial acini grown in three-dimensional basement membrane cultures. *Methods* **30**, 256-268 (2003).
32. Antoniewicz, M.R., Kelleher, J.K. & Stephanopoulos, G. Accurate assessment of amino acid mass isotopomer distributions for metabolic flux analysis. *Analytical Chemistry* **79**, 7554-7559 (2007).
33. Fernandez, C.A., Des Rosiers, C., Previs, S.F., David, F. & Brunengraber, H. Correction of ¹³C mass isotopomer distributions for natural stable isotope abundance. *J Mass Spectrom* **31**, 255-62 (1996).
34. Richardson, A.L. et al. X chromosomal abnormalities in basal-like human breast cancer. *Cancer Cell* **9**, 121-132 (2006).
35. Hoek, K. et al. Expression profiling reveals novel pathways in the transformation of melanocytes to melanomas. *Cancer Research* **64**, 5270-5282 (2004).
36. Rhodes, D.R. et al. ONCOMINE: A cancer microarray database and integrated data-mining platform. *Neoplasia* **6**, 1-6 (2004).

Supporting Information

Supplementary Table 1 – Measured peaks in [^1H , ^{13}C] HSQC spectra

Supplementary Table 2 – Statistics of *PHGDH* amplification across cancer types

Supplementary Table 3 – Metabolite intensities in control (shPHGDH) and knockdown (shPHGDH) Sk-Mel28 cells

Supplementary Table 4 – PHGDH statistical associations and references for breast cancer tumor microarray data sets

Supplementary Figure 1 - Time course of glucose flux into de novo serine biosynthesis

- a.) Labeling of [$\text{U-}^{13}\text{C}$] L-serine in HEK293T cells after 0,5,10,15 and 30 minutes of [$\text{U-}^{13}\text{C}$] glucose media replacement quantified by LC/MS. Ratio of ^{13}C L-serine to ^{13}C L-serine at time zero is plotted. Serine signal appears between 5 and 10 minutes.
- b.) GC/MS measurement of relative incorporation of [$\alpha\text{-}^{15}\text{N}$] Glutamine into amino acids in HEK293T cells. Pool sizes of relative incorporation of amino acids are shown in a pie chart.

Supplementary Figure 2 - *PHGDH* copy number gain in Melanoma

150 Melanoma samples sorted by intensity at the *PHGDH* genomic locus at 1p12. 39% contain copy number gain exhibiting the highest frequency of occurrence in cancer subtypes.

Supplementary Figure 3 - PHGDH protein expression in human melanoma

- a.) Immunohistochemistry (IHC) of $n = 381$ samples human tissue samples in a melanoma collection. Samples were scored from 0 (no expression) to 3 (high expression) and representative images are shown. Nuclei are shown in blue (hematoxylin) and PHGDH antibody is shown in brown (3-3'-Diaminobenzidine [DAB]).
- b.) Statistics of PHGDH expression according to scoring scheme in a.). Number of samples N that stain for each score and percentage values % are shown.
- c.) Representative image of interphase FISH analysis showing disomy of PHGDH (green) and pericentromeric probe (red) in a representative sample from the tissue microarray.

Supplementary Figure 4 - Analysis of PHGDH expression in human breast cancer microarrays

Associations of PHGDH expression with clinical parameters and prognosis in human breast cancer tumor microarray data sets. Test statistics are based on centroids and references are described in supplementary table 4.

Supplementary Figure 5 - Analysis of PHGDH protein expression in human breast cancer

a.) IHC staining of a set of $n = 106$ human breast tumors. PHGDH is shown in brown (DAB) and nuclei are blue (Hematoxylin). Representative images from expression scores ranging from 0 (no expression) to 3 (high expression) are shown. b.) Average mRNA expression for each IHC expression score.

Supplementary Figure 6 - Association of PHGDH protein expression in human breast cancer with clinical parameters and breast cancer subtypes

Overlay of PHGDH expression score (0 - green, 1 - yellow, 2 - orange, and 3 - red) with previously defined clinical parameters. Color correspondence of each clinical parameter is shown in the legend.

Supplementary Figure 7 - Characterization of metabolism and acinar morphogenesis in MCF-10a cells

a.) Growth assay of stable human breast cancer cell lines containing shGFP or shPHGDH. Relative cell numbers for shGFP and shPHGDH normalized to shGFP are plotted for each cell line (BT-20, Sk-BR-3, MCF-7, and MCF-10A). BT-20 cells contain 1p12 copy number gain. Sk-BR-3 and MCF-7 cells do not have 1p12 copy number gain. MCF10a cells are also shown for comparison. Error bars were obtained from the standard deviation of $n = 3$ independent measurements. b.) Ratio of integrated intensities (fold change), of PHGDH knockdown (shPHGDH) over control (shGFP) plotted for glycolytic intermediates. c.) Labeling of [U-13C] PEP after 0,5,10,15 and 30 minutes of [U-13C] glucose media replacement. No labeling of pSER was observed. Ratios of ^{13}C pSER at time zero to ^{13}C PEP (red, circles) and pSER (blue, squares) are plotted. A baseline noise level of $1\text{e}4$ was chosen. d.) Fold change in serine and glycine synthesis relative to no doxycycline treatment in MCF-10a cells (synthesis(/-Dox)) in the absence (-Dox ($0\mu\text{g/ml}$), red) and presence (+Dox ($1\mu\text{g/ml}$), blue) measured by GC/MS with relative incorporation of [$\alpha\text{-}^{15}\text{N}$] Glutamine into Serine (left) and Glycine (right). e.) Quantitation of acinar filling for $1\mu\text{g/ml}$ doxycycline with PHGDH construct (+DOX, PHGDH) ($N=69$), and $1\mu\text{g/ml}$ doxycycline with PHGDH mutant (V490M) construct (+DOX, V490M) ($N=74$) Dox. Each acini was scored as filled, mostly filled, mostly clear, and clear and the frequencies of each score are shown. Quantitation was obtained from multiple ($n=3$) independent measurements.

Methods

PHGDH cloning

Human *PHGDH* cDNA fragment was isolated with EcoRV and NotI from *PHGDH*/pSport6 (Openbiosystems MHS1010-73507), and cloned into the blunted BamHI and NotI sites of a pLv_x-Tight-Puro (Clontech) tetracycline inducible vector.

PHGDH RNA interference

shRNA hairpins in lentiviral vector plasmids pLKO.1 were purchased from open biosystems (<http://www.openbiosystems.com>). RNA interference was obtained using *PHGDH* targeting sequences (sh*PHGDH*) (TRCN0000028548) CCGGAGGTGATAACACAGGGAACATCTCGAGATGTTCCCTGTGTTATCACCTTTTTT and (TRCN0000028545), CCGGCTTAGCAAAGAGGAGCTGATACTCGAGTATCAGCTCCTCTTTGCTAAGTTTTT. A control hairpin in pLKO.1 vector was used targeting GFP (shGFP). HEK293T cells were transfected with pLKO.1 vectors and lenti-viral packaging vectors. All cell lines were infected using standard protocols. Selection under 2µg/ml puromycin was carried out at least two days prior to experiments.

Cell lysis, western blot, and Immunohistochemistry analysis

Exponentially growing cells were first washed with cold PBS and lysed with RIPA buffer (10 mM Tris (7.5), 150 mM NaCl, 1% Nonidet P-40, 1% Deoxycholic acid, 0.1% SDS, and 4 µg/mL each of pepstatin, leupeptin, 4-(2-Aminoethyl) benzenesulfonyl fluoride hydrochloride) and aprotinin, a phosphatase inhibitor cocktail (ThermoScientific) and 1mM DTT. Lysates were centrifuged at 14,000 rpm at 4°C for 30 minutes and supernatant retained. Protein concentration was determined with Bradford assay (BioRad). Mouse monoclonal *PHGDH* antibody was purchased from Santa Cruz (sc-100317) and mouse monoclonal beta actin (abCam ab8226) was used as a loading control. Both mouse anti-PSAT antibody (Novus) and rabbit anti-PSPH antibody (Sigma) were used at dilutions of 1:1000. *PHGDH* antibody was used at 1:500 dilution and incubated at 4°C overnight with 5% dry milk in Tris-buffered saline (0.05% Tween). Beta actin antibody was used at a 1:10000 dilution. Secondary antibodies conjugated to Horseradish Peroxidase were used at 1:10000 dilution. Western blots were developed using chemiluminescence. Quantitation was carried out using ImageJ software. For Immunohistochemistry, mouse monoclonal *PHGDH* antibody was purchased from Santa Cruz (sc-100317) and used at 1:15 dilution. Antibody specificity was first validated using paraffin-embedded cell blocks obtained from shGFP and sh*PHGDH* expressing cell lines. All IHC staining was carried out using a Dako Envision (K4006) IHC kit with hematoxylin nuclear counterstain and 3-3'-Diaminobenzidine [DAB] antibody stain.

Cell culture

The T.T cell line was a gift from Anil Rustgi. All human melanoma cell lines were obtained as gifts from Lynda Chin. All other cell lines were obtained from ATCC. HEK293T, SkBr3, MCF7, and T.T. cells were grown DMEM (Mediatech), 10% FBS, and antibiotics (Penicilin/Streptomycin, Invitrogen). H1299 cells were grown in RPMI (Mediatech), 10% FBS, and antibiotics. All human melanoma cell lines were cultured as previously in RPMI (Mediatech) with 10% FBS and antibiotics. BT20 cells were cultured in MEM (Mediatech), 10% FBS, and antibiotics. Early passage MCF-10a cells were cultured according to a protocol previously established using DMEM/F12(Mediatech), 5% Horse Serum, antibiotics supplemented with Insulin, EGF, Hydrocortisone, and Cholera Toxin³¹. Growth media contained the standard concentrations of glutamine but was not supplemented with additional glutamine.

NMR Sample Preparation, spectroscopy, data analysis

10⁸ exponentially growing HEK293T, H1299 and MCF-10a cells growing in basal growth media with dialyzed serum were harvested and metabolites were extracted in 50mL of 80% Methanol (v/v) at dry ice temperatures. Cells were incubated with [U¹³C]-glucose (Cambridge Isotope Laboratories) replaced at 25mM and incubated 24 hrs prior to harvesting. Fresh media were added 2 hours prior to the experiment. Lysates were centrifuged at 10,000g for 30 minutes at 4°C and supernatant was stored. Methanol was first evaporated at cold temperature under vacuum with rotational evaporation and samples were subsequently lyophilized. Samples were prepared for NMR spectroscopy by resuspending the lyophilized material in 700 µl of sample buffer, containing 50mM NaPO₄ (pH=7.0) and 2mM DSS (as an internal standard and chemical shift reference). The samples were immediately transferred into 5mm, 7" NMR tubes (Wilmad lab glass) for data acquisition.

All NMR spectra were acquired on a Bruker 500MHz spectrometer (Bruker, Inc., Billerica, MA.) using a 5mm triple resonance (H, C, N) Cryoprobe. The sample temperature was 25 degrees centigrade for all samples. Two-dimensional 1H-13C HSQC spectra with sensitivity enhancement were acquired with spectral widths of 12000 and 9048Hz in the direct and indirect dimensions, respectively. 1024 complex data points were acquired in the direct dimension, and 256 complex points were acquired in the indirect dimension in a linear fashion, with a subsequent 256 complex points being acquired with a non-uniform random sampling scheme. The total acquisition time for the indirect dimension was 113 milliseconds. 64 dummy scans were collected prior to the first increment, and 16 scans were acquired per increment.

The resulting HSQC spectra were processed using NMRpipe. A zero order phase correction in the directly detected dimension was used. Spectra were then

extracted in ascii format and peaks from 0-10 ppm in the proton dimension and 20-160 ppm in the carbon dimension were considered. This resulted in 1704 data points in the direct dimension and 423 data points in the indirectly detected dimension. The resulting intensities at each data point were then binned using an eight-fold reduction in the proton dimension and a two-fold reduction in the carbon dimension. The intensities at each point in the resulting 213 x 206 lattice were then computed and a baseline value of 5e6 was defined that corresponded to a value above the signal to noise level and each bin exhibiting sum intensity less than that of the baseline was set to the baseline. Bins in the region of the spectra containing the water line (4.60 – 4.75 ppm) were omitted. The resulting bins that displayed at least a two-fold increase in the intensity relative to the noise level were considered. Individual metabolite assignments were carried out using the Human Metabolome Database (HMDB). Computer code was written in the PERL interpreting language. Zscores (i.e. intensities in standard units) were computed in Matlab. ¹³C Glycine peaks were integrated separately using the Sparky software package (www.cgl.ucsf.edu/home/sparky/). Peak intensities were computed using gaussian integration and error bars obtained from RMS residuals.

Targeted Liquid-Chromatography Mass Spectrometry (LC/MS)

10⁶ cells exponentially growing in basal media with dialyzed serum were harvested in 3mL 80% v/v methanol at dry ice temperatures. Fresh media was added 24 hours and 2 hours prior to the experiment. Insoluble material in lysates was centrifuged at 4000RPM for 15 minutes and resulting supernatant was evaporated using a refrigerated speed-vac. Samples were resuspended using 20μL HPLC grade water for mass spectrometry. 10μL were injected and analyzed using a 5500 QTRAP triple quadrupole mass spectrometer (AB/MDS Sciex) coupled to a Prominence UFLC HPLC system (Shimadzu) via selected reaction monitoring (SRM) of a total of 249 endogenous water soluble metabolites for analyses of samples. Some metabolites were targeted in both positive and negative ion mode for a total of 298 SRM transitions. ESI voltage was 5000V in positive ion mode and –4500V in negative ion mode. The dwell time was 5 ms per SRM transition and the total cycle time was 2.09 seconds. Samples were delivered to the MS via normal phase chromatography using a 2.0 mm i.d x 15 cm Luna NH2 HILIC column (Phenomenex) at 285 μL/min. Gradients were run starting from 85% buffer B (HPLC grade acetonitrile) to 42% B from 0-5 minutes; 42% B to 0% B from 5-16 minutes; 0% B was held from 16-24 minutes; 0% B to 85% B from 24-25 minutes; 85% B was held for 7 minutes to re-equilibrate the column. Buffer A was comprised of 20 mM ammonium hydroxide/20 mM ammonium acetate in 95:5 water : acetonitrile. Peak areas from the total ion current for each metabolite SRM transition were integrated using MultiQuant v1.1 software (Applied Biosystems). Glucose-13C labeled samples were run with 249 total SRM transitions (40 in positive ion mode and 209 in negative ion mode) with a total cycle time of 0.464 seconds.

Isotope labeling and kinetic profiling

Basal media using dialyzed serum without glucose was supplemented with [U¹³C]-glucose (Cambridge Isotope Laboratories) to a concentration equivalent to the concentration suggested by ATCC protocol. Fresh media was added two hours prior to the kinetics experiment. Media was replaced by equivalent [U¹³C]-glucose labeled media and cells quickly harvested at given time points using the above mentioned protocol. Steady-state [U¹³C]-glucose labeling involved labeling cells for 12 hours prior to metabolite extraction. Samples were prepared as described above. Data analysis was performed in Matlab.

Gas-Chromatography Mass Spectrometry (GC/MS)

Cells were cultured in 6 well plates before replacing medium with DMEM containing 10% dialyzed FBS and either [U-¹³C]glucose + unlabeled glutamine or [α -¹⁵N]glutamine and unlabeled glucose. After 24 hours, cells were rinsed with 1 ml ice cold PBS and quenched with 0.4 ml ice cold methanol. An equal volume of water was added, and cells were collected in tubes by scraping with a pipette. One volume of ice cold chloroform was added to each tube, and the extracts were vortexed at 4°C for 30 minutes. Samples were centrifuged at 14,000 *g* for 5 minutes, and the aqueous phase was transferred to a new tube for evaporation under nitrogen airflow.

Derivatization and GC/MS measurements

A two-step derivitization method was used as previously described³². Dried polar metabolites were dissolved in 20 μ l of 2% methoxyamine hydrochloride in pyridine (Pierce) and held at 37°C for 1.5 hours. After dissolution and reaction, tert-butyldimethylsilyl (TBDMS) derivatization was initiated by adding 30 μ l N-methyl-N- (tert-butyldimethylsilyl)trifluoroacetamide MBTSTFA + 1% tert-butyldimethylchlorosilane TBDMCS (Pierce) and incubating at 55°C for 60 minutes. Gas chromatography/mass spectrometry (GC/MS) analysis was performed using an Agilent 6890 GC equipped with a 30m DB-35MS capillary column connected to an Agilent 5975B MS operating under electron impact (EI) ionization at 70 eV. One μ l of sample was injected in splitless mode at 270°C, using helium as the carrier gas at a flow rate of 1 ml min⁻¹. The GC oven temperature was held at 100°C for 3 min and increased to 300°C at 3.5° min⁻¹. The MS source and quadrupole were held at 230°C and 150°C, respectively, and the detector recorded ion abundance in the range of 100 – 600 *m/z*. Mass isotopomer distributions (MIDs) for serine and glycine were determined by integrating ion fragments of 390 – 398 *m/z* and 246 – 252 *m/z*, respectively. MIDs were corrected for natural isotope abundance using in house algorithms adapted from Fernandez et al.³³.

Analysis of somatic copy number alterations of PHGDH

Data processed in Matlab across 3131 total samples and 150 melanoma samples from the Broad Institute as previously compiled¹³. Heatmaps were generated in Matlab by first sorting copy number intensity at the coding region of PHGDH. False discovery rates (q-values) on chromosome 1p were computed using a background

model previously developed and plotted in Matlab. q-values for candidate oncogenes were reported as in a previous study¹³.

Cell proliferation assays

Lentiviral infection and puromycin selection was carried out under established protocols. After puromycin selection, control and knockdown cells were plated at equal densities at initial densities were normalized to the intrinsic growth rate of each cell line and seeded cells allowed to grow for three days prior to counting. Cell numbers were counted on the final day using an automated cell counter (Cellometer Auto T4, Nexcelom Bioscience) with custom morphological parameters set for each cell line. Error bars were reported using error propagation from the standard deviation of three experiments.

3-dimensional culture and confocal microscopy

To generate acini, cells were grown in reconstituted basement membrane (Matrigel) as described previously and according the protocol at <http://brugge.med.harvard.edu/>. The overlay media was changed every four days and a given concentration of doxycycline (Sigma) was added where indicated. Acini were fixed between days 25 and 28 and immunofluorescence analyses of acini was performed as described previously. The following primary antibodies were used for immunofluorescence: cleaved caspase-3 (#9661, Cell Signaling Technology) and laminin-5 (mab19562, Millipore, Billerica, MA). The golgi apparatus was detected combining antibodies to the golgi proteins GM130 (610823, BD Biosciences) and Golgin-84 (51-9001984, BD Biosciences). DAPI (Sigma-Aldrich) was used to counterstain nuclei. For examination of luminal filling, acini were imaged using confocal microscopy to visualize the centre of each structure, and then were scored as clear (~90–100% clear), mostly clear (~50–90% clear), mostly filled (~10–50% clear), or clear (~0–10% clear).

Fluorescence *in-situ* hybridization (FISH).

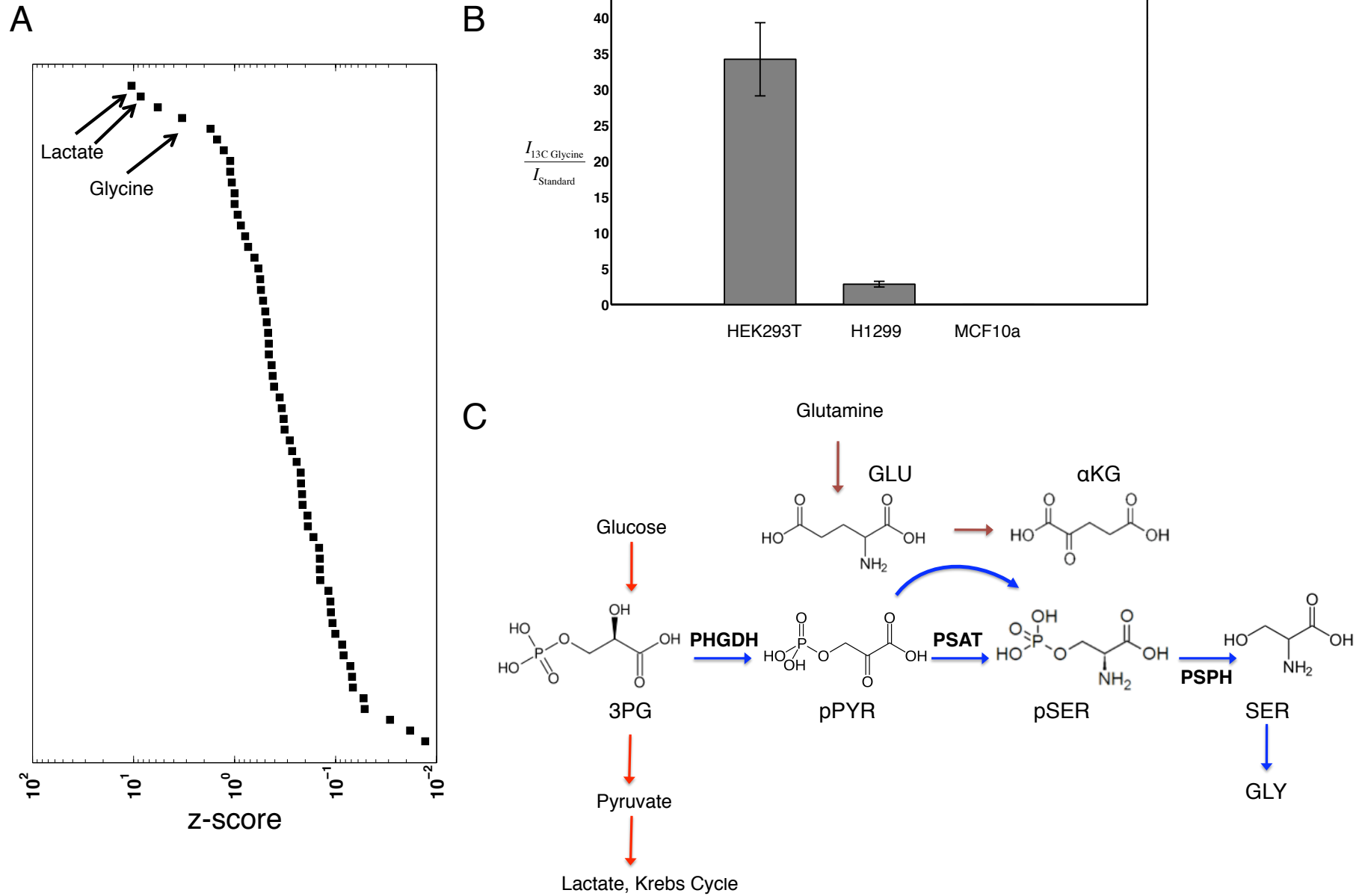
Cultured cell lines were harvested at 75% confluence and metaphase chromosome spreads were produced using conventional cytogenetic methods. Human melanoma tissue arrays were first heated to remove paraffin. Slides were aged overnight at 37°C, dehydrated by successive two minute washes with 70%, 80%, 90% and 100% ethanol, air-dried and then hybridized to DNA probes as described below. The following DNA probes were co-hybridized: RP11-22F13 (labeled in SpectrumGreen), which maps to 1p12 and includes *PHGDH*, and the D1Z5 alpha-satellite probe (SpectrumOrange; Abbott Molecular, Inc.), which maps to 1p11.1-q11.1. The RP11-22F13 BAC clone was obtained from CHORI (www.chori.org), direct-labeled using nick translation, and precipitated using standard protocols. Final probe concentration was 100ng/ul. The final concentration used for the commercial probes followed manufacturer's recommendations. The tissue sections and probes were co-denatured at 80°C for 5 min, hybridized at least 16 hrs at 37°C

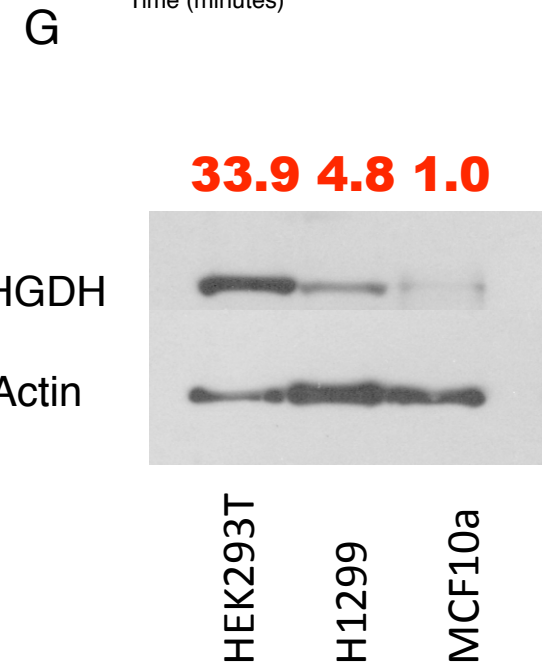
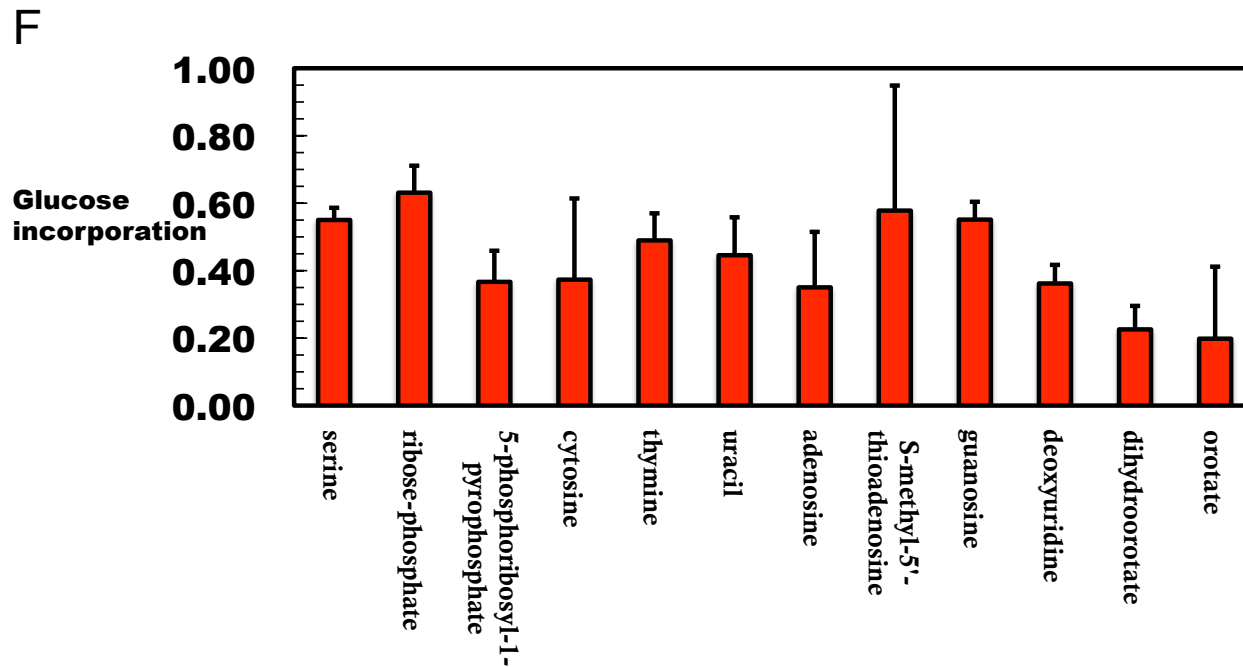
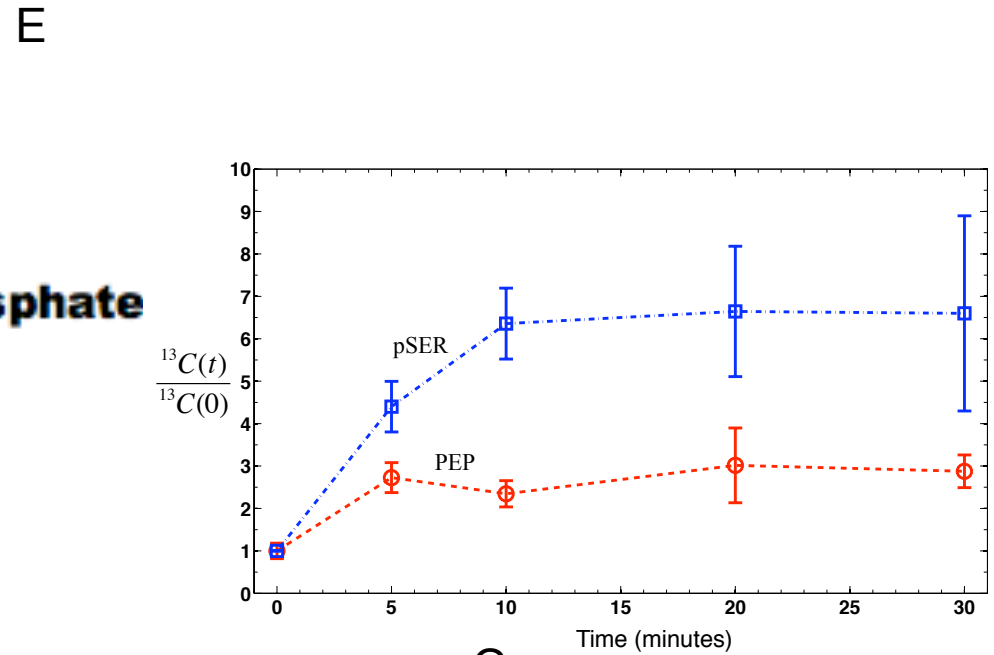
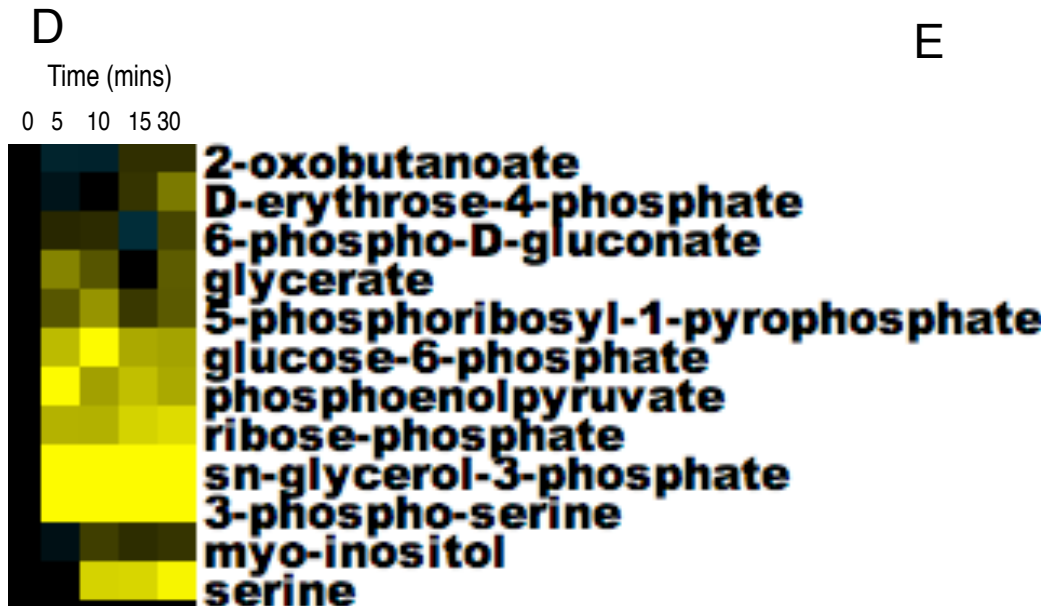
in a darkened humid chamber, washed in 2X SSC at 70°C for 10 min, rinsed in room temperature 2X SSC, and counterstained with DAPI (4',6-diamidino-2-phenylindole, Abbott Molecular/Vysis, Inc.). Slides were imaged using an Olympus BX51 fluorescence microscope. Individual images were captured using an Applied Imaging system running CytoVision Genus version 3.92.

Human tumor samples and data analysis

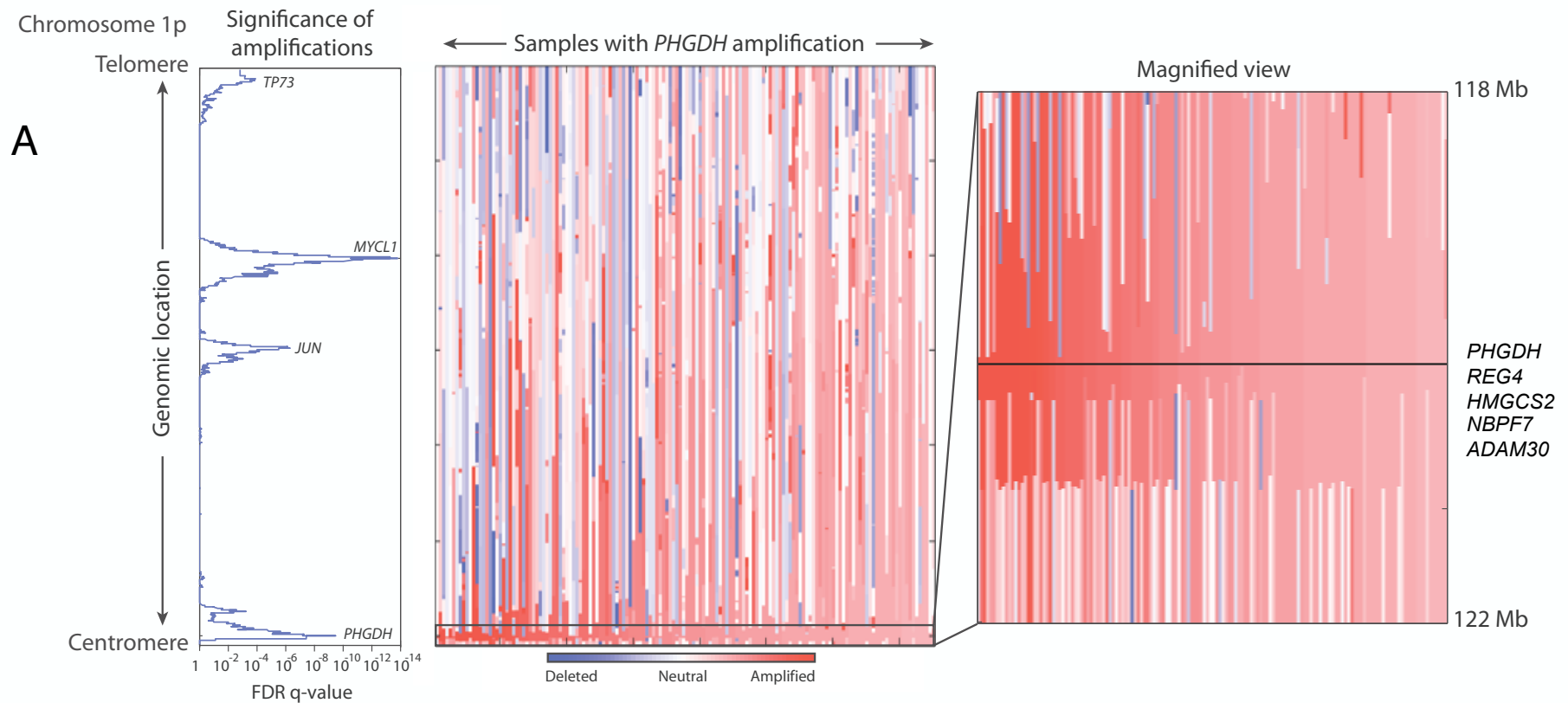
Human breast cancer patient samples were obtained from the Harvard SPORE breast tissue repository collected under DF/HCC IRB protocol #93-085. Tumor and patient characteristics, tissue microarray construction, and gene expression profiles were reported previously. Histological diagnosis and comparison with clinical parameters was based on established criteria³⁴. Human melanoma patient samples were obtained from the Yale SPORE skin cancer program and tissue microarray construction was previously reported³⁵. Histological diagnosis was based on established criteria. All bioinformatics data from human breast cancer microarrays were obtained from Oncomine using established statistics³⁶.

Locasale et al. Figure 1

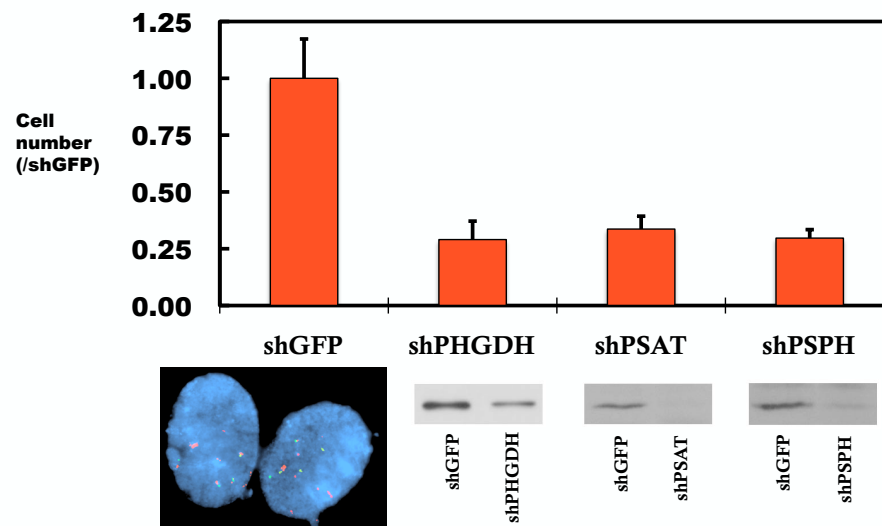




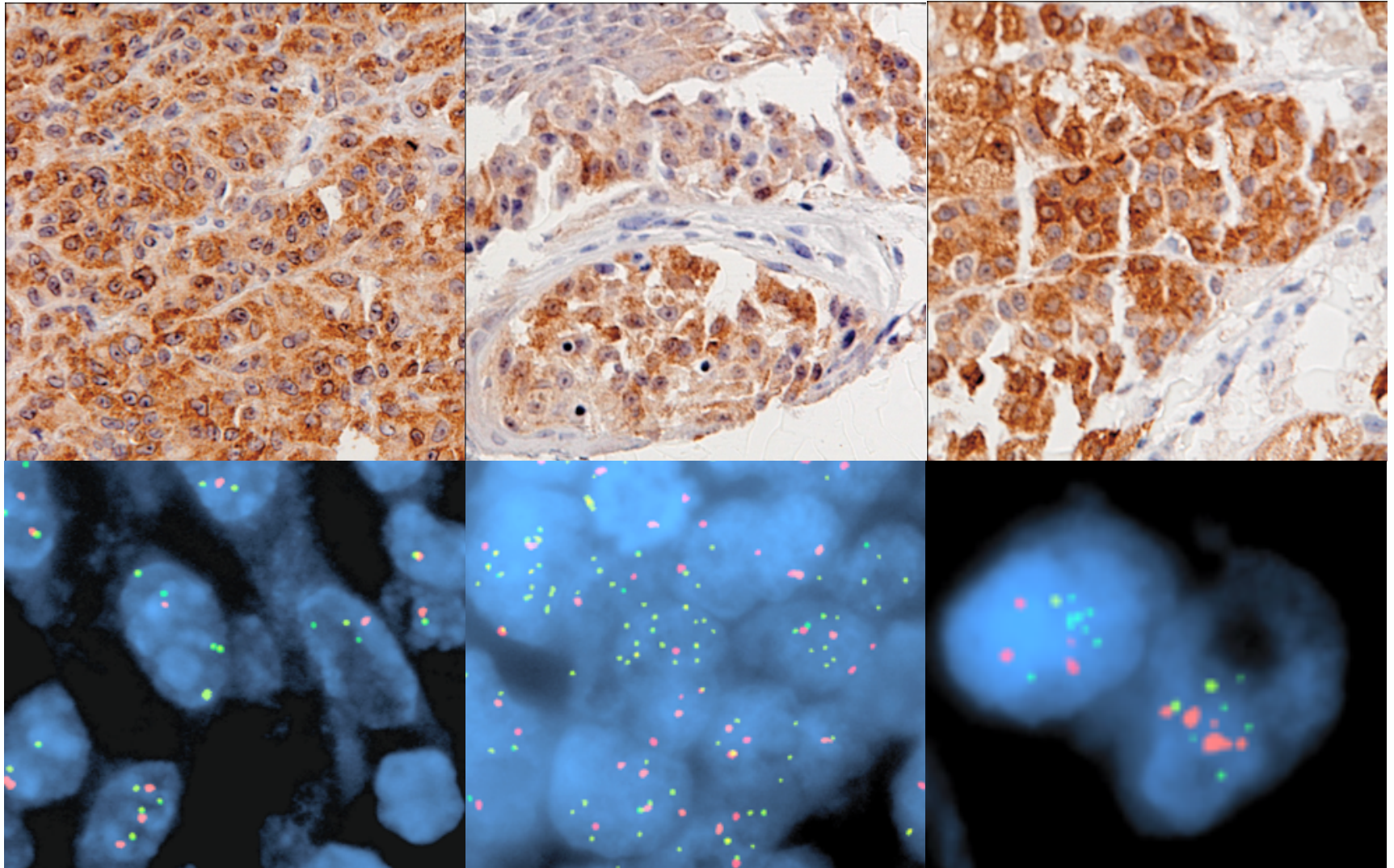
Locasale et al. Figure 2



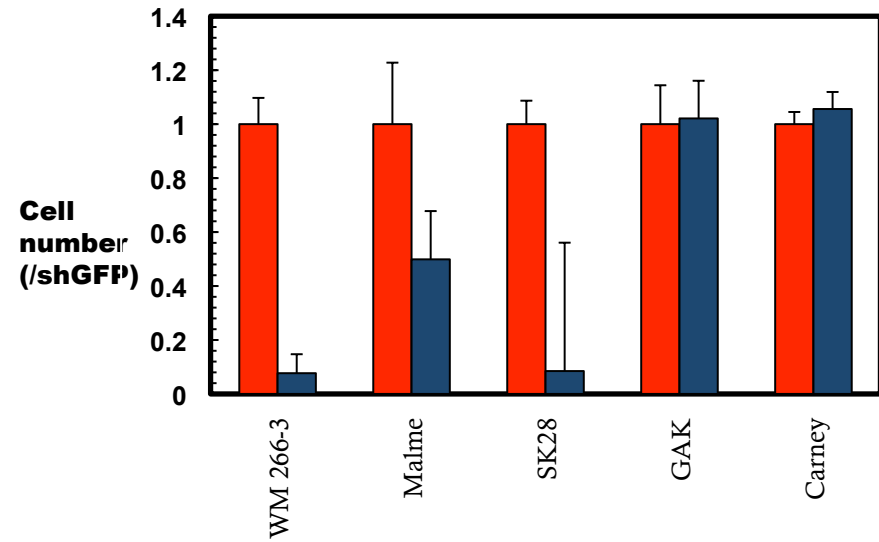
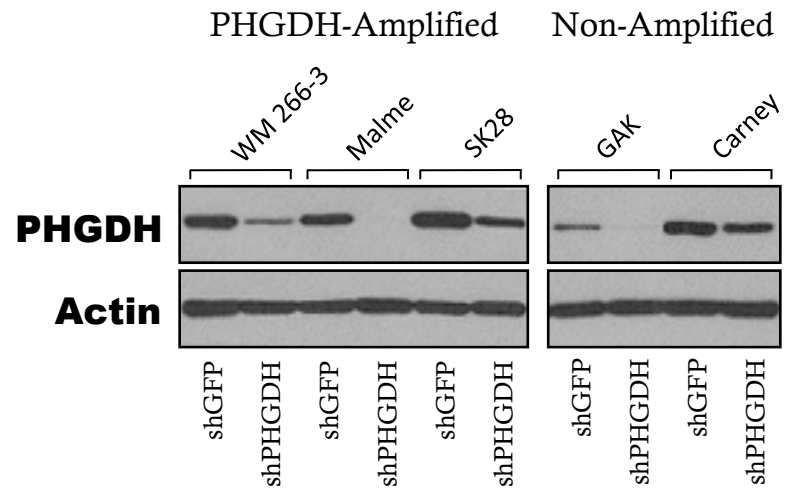
B



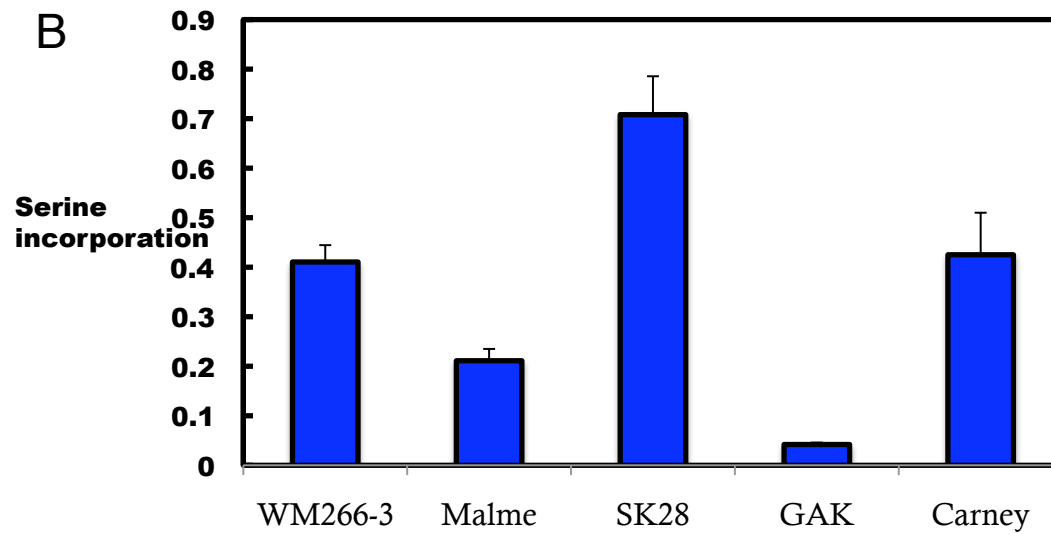
C



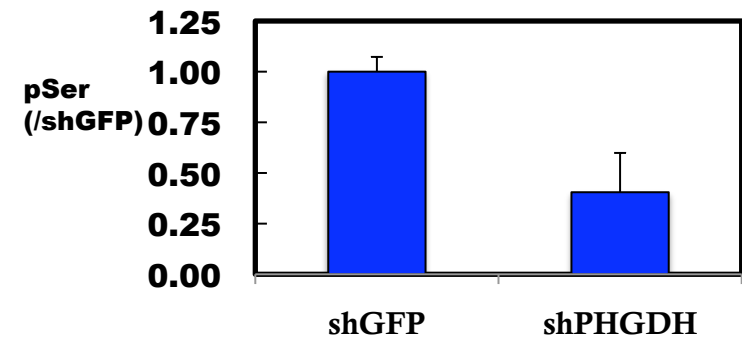
A

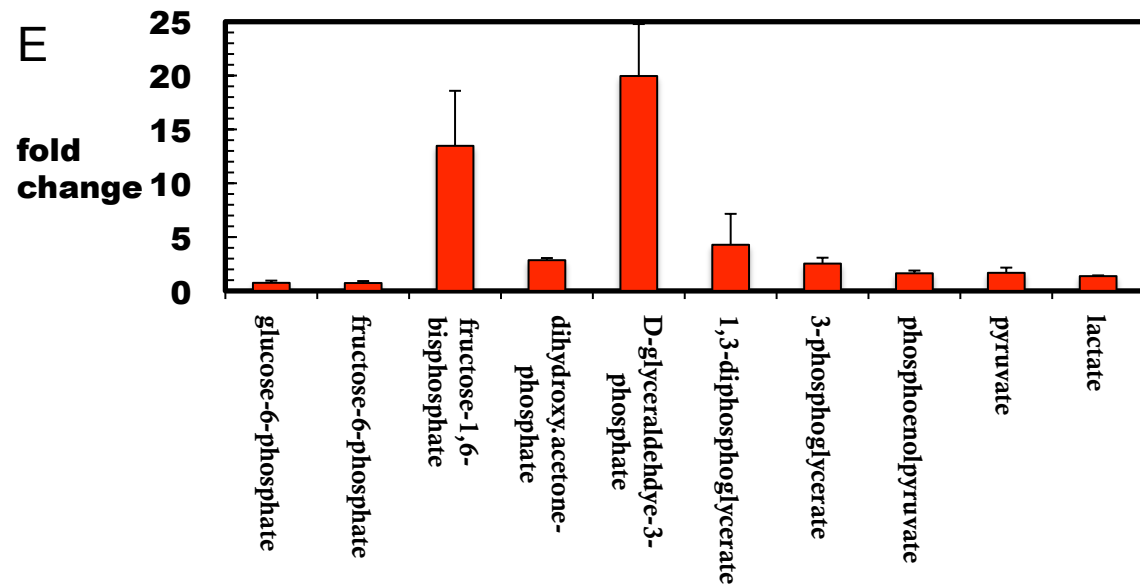
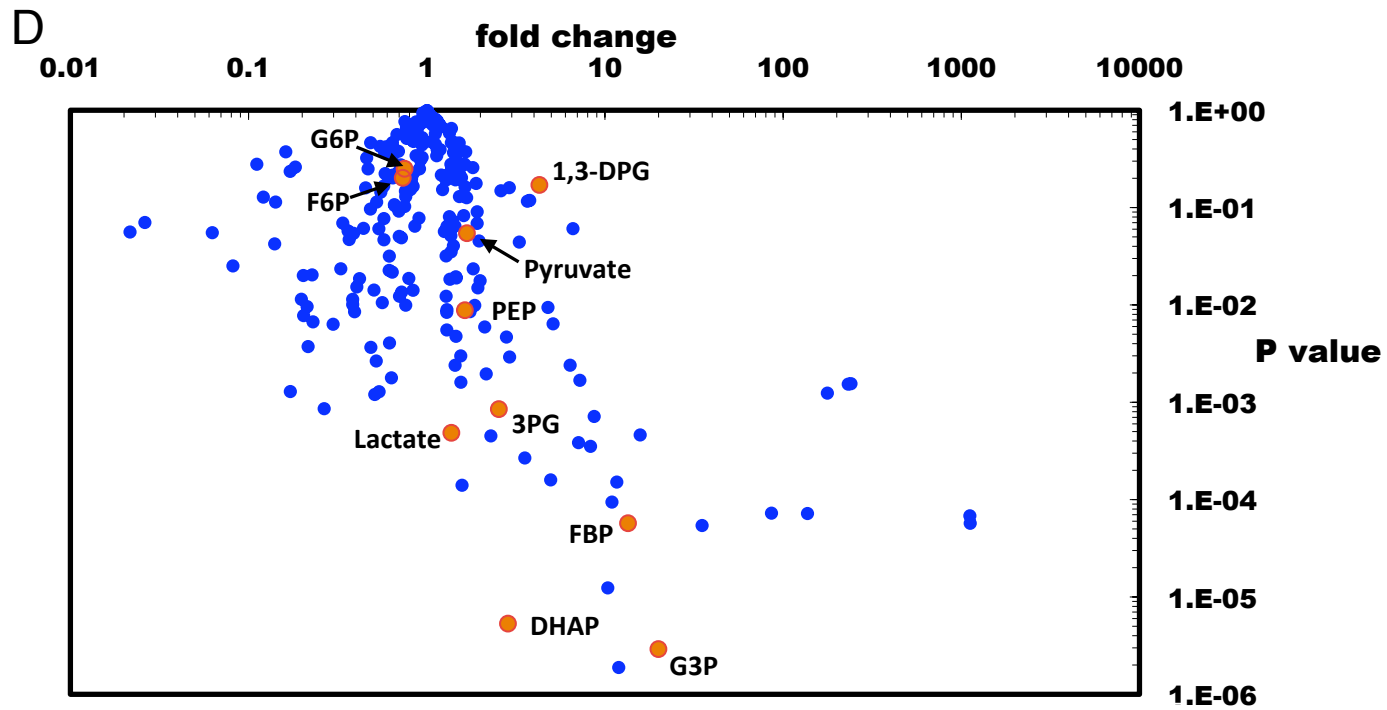


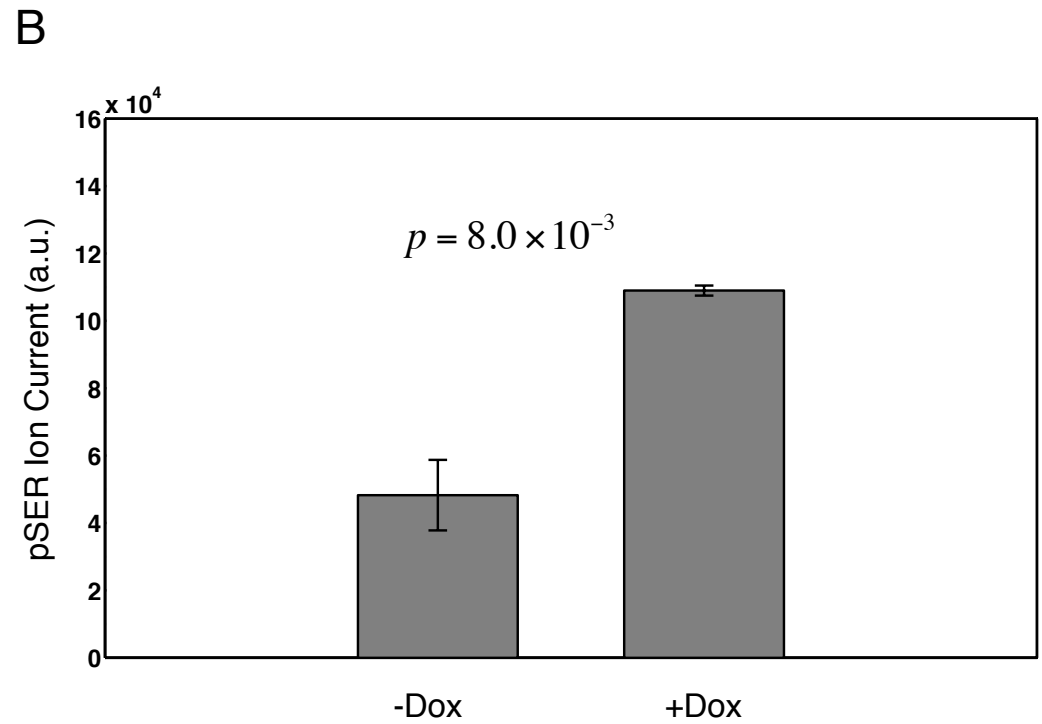
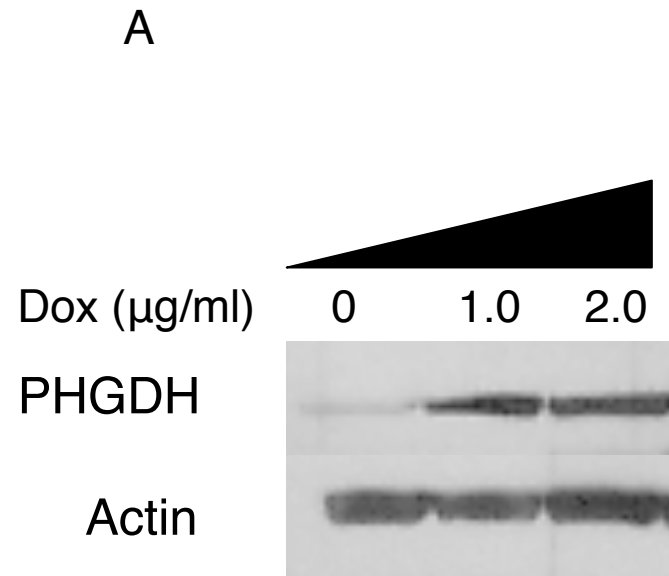
B



C

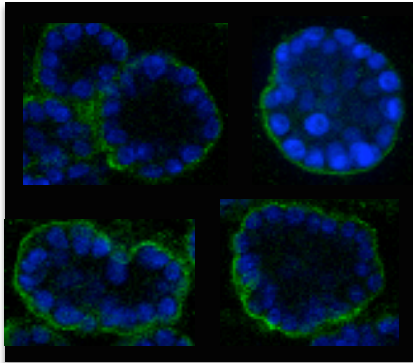






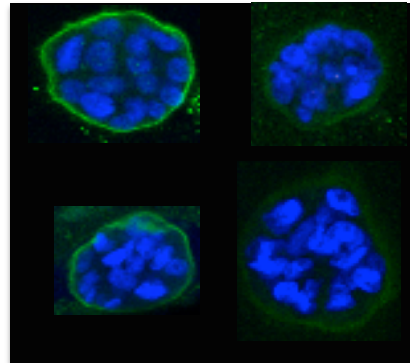
C

-DOX

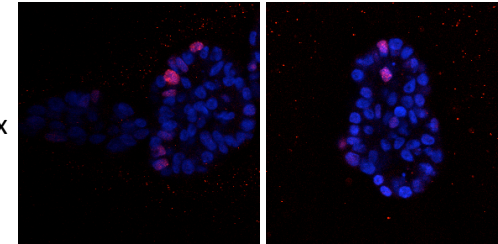


D

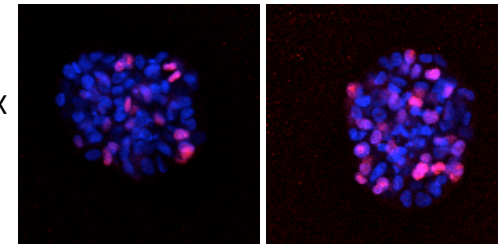
+DOX



No Dox



1 μ g/ml DOX



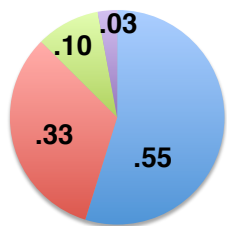
Red=Ki67

Blue=DAPI

E

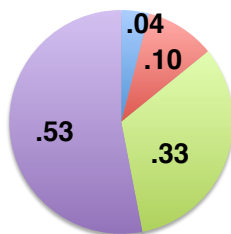
- clear
- mostly clear
- mostly filled
- filled

0 μ g/ml



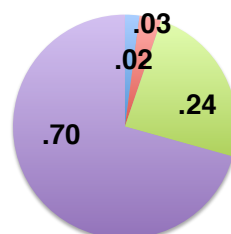
N = 239

1 μ g/ml



N = 198

2 μ g/ml



N = 191

F

